Please cite this article in press as: Cerutti et al., NAD+-Dependent Activation of Sirt1 Corrects the Phenotype in a Mouse Model of Mitochondrial Disease, Cell Metabolism (2014), http://dx.doi.org/10.1016/j.cmet.2014.04.001

Cell Metabolism
Short Article

NAD+-Dependent Activation of Sirt1 Corrects the Phenotype in a Mouse Model of Mitochondrial Disease

Raffaele Cerutti,[1,8] Eija Pirinen,[2,3] Costanza Lamperti,[1] Silvia Marchet,[1] Anthony A. Sauve,[4] Wei Li,[4] Valerio Leoni,[5] Eric A. Schon,[6] Françoise Dantzer,[7] Johan Auwerx,[2] Carlo Viscomi,[1,8,*] and Massimo Zeviani[1,8,*]
[1]Unit of Molecular Neurogenetics, The Foundation "Carlo Besta" Institute of Neurology IRCCS, 20133 Milan, Italy
[2]Laboratory for Integrative and Systems Physiology, Ecole Polytechnique Fédérale de Lausanne, Lausanne CH-1015, Switzerland
[3]Biotechnology and Molecular Medicine, A.I. Virtanen Institute for Molecular Sciences, Biocenter Kuopio, University of Eastern Finland, FI-70211 Kuopio, Finland
[4]Department of Pharmacology, Weill Cornell Medical College, New York, NY 10021, USA
[5]Laboratory of Clinical Pathology and Medical Genetics, The Foundation "Carlo Besta" Institute of Neurology IRCCS, 20133 Milan, Italy
[6]Department of Neurology, College of Physicians and Surgeons, Columbia University, New York, NY 10032, USA
[7]Biotechnologie et Signalisation Cellulaire, UMR7242 CNRS, Université de Strasbourg, ESBS, 67412 Illkirch, France
[8]MRC-Mitochondrial Biology Unit, Cambridge CB2 0XY, UK
*Correspondence: cfv23@mrc-mbu.cam.ac.uk (C.V.), mdz21@mrc-mbu.cam.ac.uk (M.Z.)
http://dx.doi.org/10.1016/j.cmet.2014.04.001

SUMMARY

Mitochondrial disorders are highly heterogeneous conditions characterized by defects of the mitochondrial respiratory chain. Pharmacological activation of mitochondrial biogenesis has been proposed as an effective means to correct the biochemical defects and ameliorate the clinical phenotype in these severely disabling, often fatal, disorders. Pathways related to mitochondrial biogenesis are targets of Sirtuin1, a NAD+-dependent protein deacetylase. As NAD+ boosts the activity of Sirtuin1 and other sirtuins, intracellular levels of NAD+ play a key role in the homeostatic control of mitochondrial function by the metabolic status of the cell. We show here that supplementation with nicotinamide riboside, a natural NAD+ precursor, or reduction of NAD+ consumption by inhibiting the poly(ADP-ribose) polymerases, leads to marked improvement of the respiratory chain defect and exercise intolerance of the Sco2 knockout/knockin mouse, a mitochondrial disease model characterized by impaired cytochrome *c* oxidase biogenesis. This strategy is potentially translatable into therapy of mitochondrial disorders in humans.

INTRODUCTION

Primary mitochondrial disorders due to impaired oxidative phosphorylation (OXPHOS) are a well-established cause of severe disability and precocious death in both children and adults (Koopman et al., 2012). No effective therapies are currently available for these conditions, but encouraging results have recently been obtained by stimulating mitochondrial biogenesis acting on either the PPAR system (Wenz et al., 2008) or the AMP-kinase (AMPK)/PGC1α axis (Viscomi et al., 2011). Importantly, these approaches can in principle be extended to several mitochondrial diseases with different genetic causes, as they do not point to the correction of a specific defect but are based on a more general strategy aimed at increasing the overall residual activity of the respiratory chain.

Additional targets able to activate the mitochondriogenic program and boost mitochondrial function are sirtuins 1–7 (Houtkooper et al., 2012), the mammalian orthologs of the yeast silent information regulator (Sir) 2 gene (Imai et al., 2000; Vaziri et al., 2001). Sirtuins have different subcellular localization, Sirt1 and Sirt6 being mainly found in the nucleus, Sirt2 in the cytosol, Sirt3–Sirt5 in mitochondria, and Sirt7 in the nucleolus. Sirtuins are important regulators of several proteins, including key metabolic players, acting as either deacetylases or ADP-ribosylases (Houtkooper et al., 2012). The most-investigated member of the family is Sirtuin1 (Sirt1), a NAD+-dependent type III nuclear deacetylase that utilizes NAD+ as a cosubstrate to remove acetyl groups from lysine residues of a target protein. Known targets of Sirt1 are the tumor suppressor p53, the myocyte-specific enhancer factor 2 (MEF2), the Forkhead box O (FOXO), and PGC1α, all of which regulate transcriptional programs related to increased mitochondrial function (Andreux et al., 2013). Sirt1 activity is directly regulated by NAD+ availability, by substrate-dependent activation, raising the hypothesis that NAD+ acts as a metabolic sensor. For instance, both NAD+ levels and Sirt1 activity increase in mammalian tissues in response to energy/nutrient stresses such as exercise (Cantó and Auwerx, 2009, 2010) and fasting (Cantó and Auwerx, 2010; Chen et al., 2008; Rodgers et al., 2005). Recent studies have shown that Sirt1 activation can prevent diet-induced obesity in mice. This effect was achieved by increasing the content of NAD+ in cells and tissues essentially through (1) dietary supplementation of suitable NAD+ precursors, such as Nicotinamide Riboside, NR (Cantó et al., 2012), or (2) inhibition of NAD+-consuming enzymes, such as the poly(ADP-ribose) polymerase 1, PARP1 (Bai et al., 2011). Here, we have tested the

Please cite this article in press as: Cerutti et al., NAD+-Dependent Activation of Sirt1 Corrects the Phenotype in a Mouse Model of Mitochondrial Disease, Cell Metabolism (2014), http://dx.doi.org/10.1016/j.cmet.2014.04.001

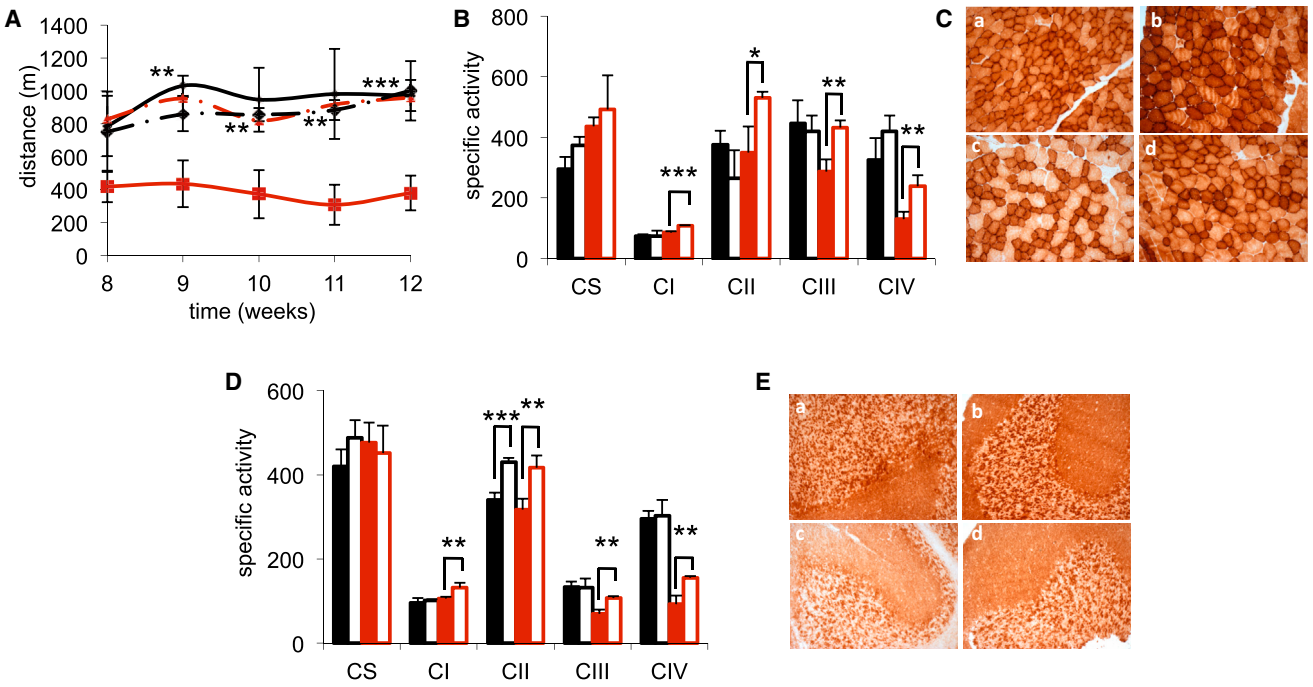

Figure 1. Characterization of *Parp1*$^{-/-}$-Sco2^{KOKI} Double Mutants

(A) Treadmill analysis of motor performance. Solid black, WT; dashed black, *Parp1*$^{-/-}$; solid red, *Sco2*^{KOKI}; dashed red, *Parp1*$^{-/-}$-*Sco2*^{KOKI}. The asterisks represent the significance levels calculate by unpaired, two-tailed Student's t test; ***p < 0.001.

(B) MRC activities (nmoles/min/mg of protein) in skeletal muscle. Solid black, WT; black outline, *Parp1*$^{-/-}$; solid red, *Sco2*^{KOKI}; red outline, *Parp1*$^{-/-}$-*Sco2*^{KOKI}. CS, citrate synthase; CI-IV, MRC complexes I–IV. Error bars represent the standard deviation (SD). Unpaired, two-tailed Student's t test; *p < 0.05; **p < 0.01; ***p < 0.001.

(C) COX staining in skeletal muscle of WT (Ca), *Parp1*$^{-/-}$ (Cb), *Sco2*^{KOKI} (Cc), and *Sco2*^{KOKI}-*Parp1*$^{-/-}$ mice (Cd). Note the increased COX staining in the double mutants. Scale bar, 100 μm.

(D) MRC activities in the brain. Color codes as in (B). Error bars represent the standard deviation (SD). Unpaired, two-tail Student's t test; **p < 0.01; ***p < 0.001.

(E) COX staining in the brain of WT (Ea), *Parp1*$^{-/-}$ (Eb), *Sco2*^{KOKI} (Ec), and *Sco2*^{KOKI}-*Parp1*$^{-/-}$ mice (Ed). Scale bar, 100 μm.

therapeutic efficacy of these strategies on a genetic mitochondrial disease model, the *Sco2* knockout/knockin (*Sco2*^{KOKI}) mouse (Yang et al., 2010). *Sco2* encodes a metallochaperone involved in the formation of the copper redox centers into nascent complex IV (cytochrome *c* oxidase, COX) (Leary et al., 2009). Mutations in this gene lead to infantile fatal encephalocardiomyopathy (Papadopoulou et al., 1999). Most of the patients carry at least one allele encoding the common mutation p.E140K, corresponding to the p.E129K mutation in the knockin murine *Sco2* allele. The second knockout allele in this animal model is functionally null (Yang et al., 2010). While homozygous knockout individuals are embryonic lethal, the *Sco2*^{KOKI} mice show a predominantly myopathic phenotype characterized by exercise intolerance and associated with ubiquitous COX deficiency.

RESULTS

Ablation of PARP1 Improves Motor Performance in Sco2^{KOKI} Mice

To test the effects of persistent increase of the NAD$^+$ pool on the *Sco2*^{KOKI} mouse, we first crossed it with a constitutive *Parp1*$^{-/-}$ mouse (de Murcia et al., 1997), which shows increased levels of NAD$^+$ in skeletal muscle (Bai et al., 2011). The *Sco2*^{KOKI}-*Parp1*$^{-/-}$ double mutants showed reduced fasting blood glucose levels, body weight and epididymal white adipose tissue (WAT) compared to *Sco2*^{KOKI} littermates, whereas no differences were observed between WT and *Parp1*$^{-/-}$ littermates (see Figure S1 available online). The endurance motor performance of *Sco2*^{KOKI}-*Parp1*$^{-/-}$ double mutants, *Sco2*^{KOKI}, *Parp1*$^{-/-}$, and WT littermates (four animals per group) was monitored weekly by a standard treadmill test for 4 weeks starting at 2 months of age. While *Sco2*^{KOKI} mice showed markedly reduced motor performance compared to WT littermates throughout the observation time, the double mutant individuals performed as well as the WT and *Parp1*$^{-/-}$ littermates (Figure 1A). Biochemically, significant reduction of complex IV activity and, to a lesser extent, complex III as well (Yang et al., 2010), was measured in skeletal muscle of *Sco2*^{KOKI} mice. In the muscle homogenate of *Sco2*^{KOKI}-*Parp1*$^{-/-}$ double mutants, these activities were comparable to that of *Parp1*$^{-/-}$ and WT littermates, whereas complex I and II activities were even higher (Figure 1B; Table S1). Accordingly, the intensity of the histochemical staining specific to COX was increased in skeletal muscle of the double mutants, compared to the *Sco2*^{KOKI} mutants (Figure 1C). The activities of complex III and IV (Figure 1D;

Table S2) were also increased in the brains of double mutants relative to *Sco2*^{KOKI} animals, but remained significantly lower than those measured in *Parp1*$^{-/-}$ and WT littermates; the histochemical reaction to COX was concordant with the biochemical data (Figure 1E).

NR Increases Motor Performance and Induces OXPHOS-Related Gene Expression in Sco2^{KOKI} Skeletal Muscle

To test the effects of pharmacological intervention, we first administered NR to *Sco2*^{KOKI} mice and WT littermates (n = 4/group), as a food admix (400 mg/Kg) (Cantó et al., 2012) for four weeks. Metabolic parameters in the treated groups, including reduced blood glucose, plasma fatty acids, and epididymal WAT, mirrored those of *Parp1*$^{-/-}$ mice (Figure S2), confirming that NR, or its derivative NMN, was pharmacologically active in vivo. NR-treated *Sco2*^{KOKI} mice significantly improved their motor performance compared to the vehicle-treated *Sco2*^{KOKI} group, rapidly achieving the levels of motor endurance displayed by treated and untreated WT mice (Figure 2A), which showed no difference to each other. These results suggest that NR treatment increases mitochondrial function in the *Sco2*^{KOKI} mice through NAD$^+$ activation of Sirt1 (Cantó et al., 2012). Accordingly, the NAD$^+$/NADH ratio was significantly increased (Figure 2B), and the ratio between acetylated and total FOXO1, a direct target of Sirt1, was clearly reduced (Figure 2C) in skeletal muscle of NR-treated versus vehicle-treated *Sco2*^{KOKI} and WT animals. We did not observe differences in mtDNA content (data not shown) and citrate synthase (CS) activity (Figure 2F), but mRNA levels of several genes related to either fatty acids oxidation (FAO), including ACOX and CD36, or oxidative phosphorylation (COXI, COXII, COXIV, COXVa) were significantly increased in NR-treated versus vehicle-treated *Sco2*^{KOKI} but not in WT animals (Figure 2D). TFAM, a key factor of mtDNA transcription, was also increased, and UCP3 and PDK4, which were downregulated in *Sco2*^{KOKI} mice, returned to control levels upon NR treatment. As expected, we found no change in transcripts specific to PGC1α, which is activated posttranscriptionally by Sirt1, and to two PGC1α partners, NRF1 and NRF2. Accordingly, western blot immunovisualization demonstrated increased levels of several nuclear- and mitochondrial-DNA-encoded OXPHOS-related proteins in NR-treated versus vehicle-treated skeletal muscle samples (Figure 2E). In the same specimens, mitochondrial respiratory chain activities were significantly increased (Figure 2F; Table S3) in NR-treated versus vehicle-treated *Sco2*^{KOKI} mice, but not in WT animals. The histochemical staining for COX reflected the biochemical results (Figure 2G).

In both *C. elegans* and mammalian cells, NR-dependent Sirt1 activation can induce the mitochondrial unfolded protein response (mtUPR), a stress-response protective mechanism which can improve mitochondrial function (Durieux et al., 2011; Mouchiroud et al., 2013). We found that the mtUPR-specific transcripts *Clpp*, *Hsp60*, and *Sod2* were significantly increased in muscle samples of NR-treated *Sco2*^{KOKI} mice, whereas *Sod3*, which is unrelated to mtUPR, was unchanged (Figure 2H).

No effect of the NR treatment was observed on the mitochondrial respiratory chain activities in the brain of our animals (Table S4).

PARP1 Inhibitors Induce Mitochondrial Function in Skeletal Muscle and Brain

Next, we administered a pan-PARP inhibitor (MRLB-45696, IC_{50} for PARP < 1 nM; Pirinen et al., 2014, in this issue of *Cell Metabolism*) at 50 mg/Kg as a food admix for 4 weeks. In MRLB-45696-treated *Sco2*^{KOKI} mice, we observed metabolic effects similar to those of NR treatment (Figure S3). Weekly treadmill tests showed progressive increase, up to normal, of the motor endurance in MRLB-45696-treated *Sco2*^{KOKI}, whereas no change was seen in WT mice (Figure 3A). The NAD$^+$/NADH ratio was significantly increased in treated versus untreated WT, but not in the *Sco2*^{KOKI}, animals (Figure 3B), whereas the acetylated/total FOXO1 ratio was reduced in both treated groups (Figure 3C), indicating activation of Sirt1 by MRLB-45696.

Similar to NR, MRLB-45696 increased the mRNA expression levels of OXPHOS- and FAO-related genes in both *Sco2*^{KOKI} and WT mice, whereas mtDNA content (data not shown) and CS activity (Figure 3F) remained unchanged. In treated *Sco2*^{KOKI} but not in WT animals, western blot analysis showed increased content of mitochondrial respiratory chain subunits (Figures 3D and 3E), which was paralleled by significantly increased mitochondrial respiratory chain activities (Figure 3F; Table S3). Histochemistry for COX showed increased staining in treated versus vehicle-treated *Sco2*^{KOKI} mice (Figure 3G). Again, we found that expression of the mtUPR genes *Hsp60*, *Clpp*, and *Sod2* was significantly increased, unlike the mtUPR-unrelated gene *Sod3* (Figures 3H and 3I).

In contrast to the NR treatment, the MRLB-45696 treatment determined significant increase of COX transcripts (Figure 4A), and respiratory chain activities in the brain (Figure 4B; Table S4). The intensity of COX staining was increased as well (Figure 4C).

Similar results were obtained in both skeletal muscle and brain by using PJ34, a commercially available pan-PARP inhibitor (Figures S3 and S4; Table S4).

DISCUSSION

The NAD$^+$ pool is set by the balance between de novo and salvage biosynthetic pathways and utilization by NAD$^+$-consuming enzymes. NAD$^+$ is synthesized de novo from tryptophan, but the main source of NAD$^+$ is from salvage pathways (Houtkooper et al., 2010). These require the uptake of other NAD$^+$ precursors from the diet, including NR. Upon its entry in the cell, NR is phosphorylated by NR kinases into nicotinamide mononucleoside (NMN), which is then converted to NAD$^+$ by NMN adenylyltransferase (Bieganowski and Brenner, 2004). NAD$^+$ biosynthesis and cellular levels are also controlled by a circadian clock related to the feeding/fasting cycle. For example, in the mitochondrial compartment NAD$^+$ levels regulate Sirtuin 3, a deacetylase targeting respiratory chain subunits (Peek et al., 2013), while in the nucleus NAD$^+$ is a substrate of both Parp1 and Sirt. Parp1, the highest consumer of NAD$^+$ in mammalian tissues, is activated upon binding to damaged or abnormal DNA (Durkacz et al., 1980) and catalyzes the formation of poly(ADP-ribose) polymers (PAR) using NAD$^+$ as a substrate, onto different acceptor proteins, including Parp1 itself (Adamietz, 1987).

Ablation of the *Parp1* gene, supplementation of NR or administration of Parp inhibitors (PARPi) can expand the NAD$^+$ pool

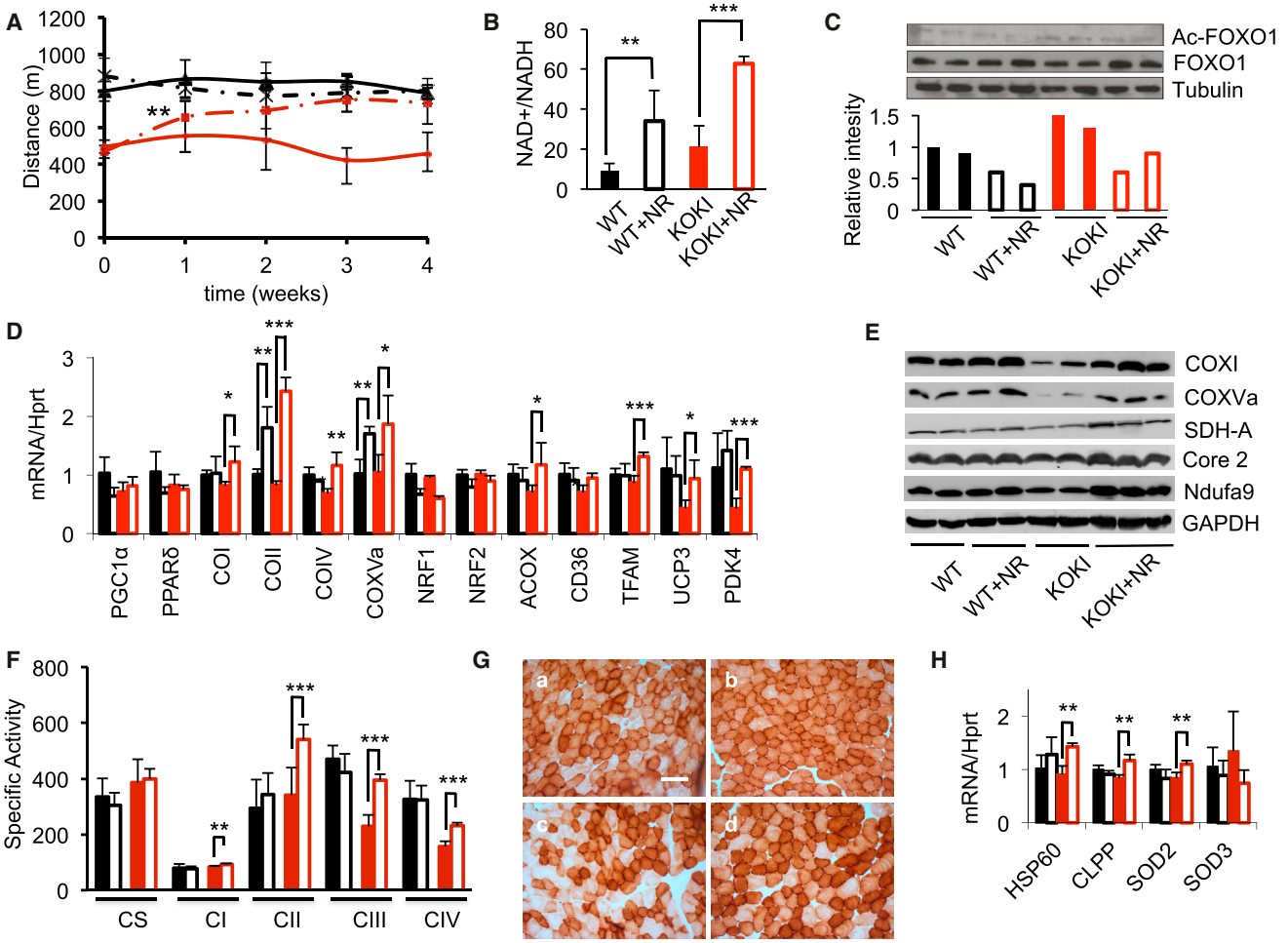

Figure 2. Effect of NR in Skeletal Muscle

(A) Treadmill analysis of motor performance. Solid black, vehicle-treated WT; dashed black, NR-treated WT; dashed red, vehicle-treated *Sco2*^{KOKI}; solid red, vehicle-treated *Sco2*^{KOKI}; dashed red, NR-treated *Sco2*^{KOKI}. Paired, two-tailed Student's t test, **p < 0.01.

(B) NAD^+ concentration in skeletal muscle. Solid black, vehicle-treated WT; black outline, NR-treated WT; solid red, vehicle-treated *Sco2*^{KOKI}; red outline, NR-treated *Sco2*^{KOKI}. Error bars represent SD. Unpaired, two-tailed Student's t test; *p < 0.05; **p < 0.01.

(C) Analysis of acetylation of FOXO1. (Upper panel) Representative western blot immunovisualization. (Lower panel) Densitometric analysis. Note that both WT and *Sco2*^{KOKI} samples showed reduced acetylation and increased total FOXO1 upon NR treatment, indicating activation of Sirt1. Tubulin was taken as loading control. Color codes as in (B).

(D) Analysis of mRNA expression of FAO- and OXPHOS-related genes in *Sco2*^{KOKI} and WT muscles of NR-treated and vehicle-treated mice. Color codes as in (B). Gene transcripts, retrotranscribed into cDNA, were normalized to the *Hprt* gene transcript, taken as a standard, and expressed as time fold variation relative to the WT. Error bars represent SD. Unpaired, two-tailed Student's t test; *p < 0.05; **p < 0.01; ***p < 0.001.

(E) Western blot immunovisualization of COX1, COXVa, SDH 70KDa, Core 2, 39 KDa complex I subunit proteins in skeletal muscle of NR-treated and vehicle-treated mice of the different genotypes. Note the increased amount of respiratory chain subunits in NR-treated *Sco2*^{KOKI} samples.

(F) MRC activities (nmoles/min/mg of protein). Color codes as in (B). CS, citrate synthase; CI-IV, MRC complexes I–IV. Error bars represent SD. Unpaired, two-tail Student's t test; **p < 0.01; ***p < 0.001.

(G) COX staining in skeletal muscles of (Ga) vehicle-treated WT, (Gb) NR-treated WT, (Gc) vehicle-treated *Sco2*^{KOKI}, and (Gd) NR-treated *Sco2*^{KOKI}. Scale bar, 100 μm.

(H) mRNA expression analysis of mtUPR genes *Hsp60*, *Clpp*, and *Sod2* in *Sco2*^{KOKI} and WT muscles of NR-treated and vehicle-treated mice. *Sod3* was taken as a non-mtUPR-related stress protein. Color codes as in (B). Gene transcripts, retrotranscribed into cDNA, were normalized to that of the Hprt gene transcript, taken as a standard, and expressed as time fold variation relative to the WT. Error bars represent SD. Unpaired, two-tailed Student's t test; **p < 0.01.

and activate sirtuins, particularly Sirt1, a master regulator of mitochondrial homeostasis. These effects can protect mice from high-fat (HF)-induced metabolic disease (Cantó et al., 2012). We have shown here that these treatments can correct the biochemical and clinical phenotype of the *Sco2*^{KOKI} mouse, a model of genetically determined mitochondrial disease. Increased transcription of genes related to both OXPHOS and mtUPR was associated with activation of oxidative metabolism, increase of mitochondrial respiratory chain activities, and normalization of the endurance motor deficit, displayed by naive *Sco2*^{KOKI} animals. Notably, these effects were hardly seen in WT littermates, suggesting that mitochondrial dysfunction sensitizes

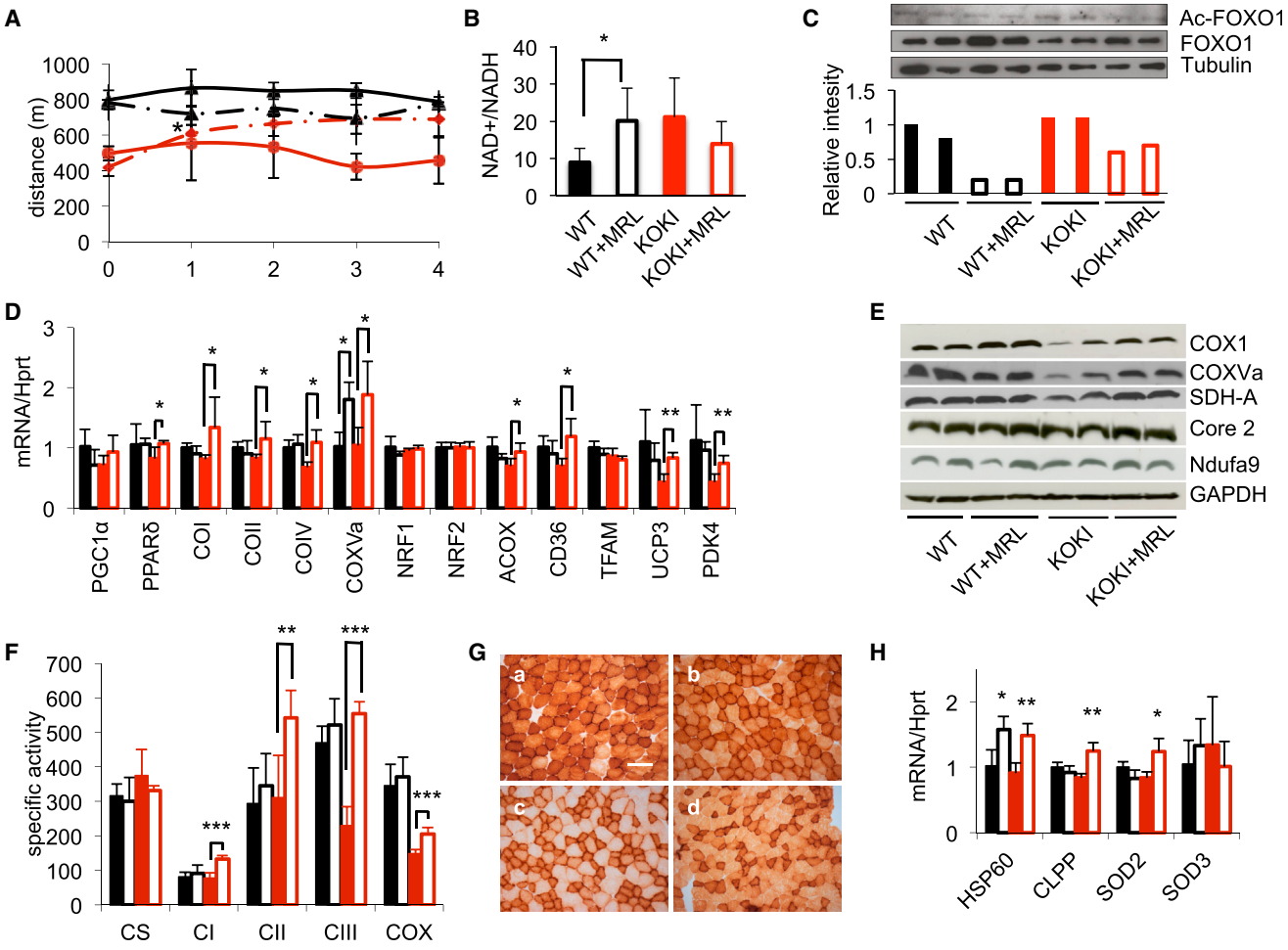

Figure 3. Effects of MRLB-45696 on the Skeletal Muscle

(A) Treadmill analysis of motor performance. Solid black, vehicle-treated WT; dashed black, MRLB-45696-treated WT; dashed red, vehicle-treated *Sco2*^{KOKI}; solid red, vehicle-treated *Sco2*^{KOKI}; dashed red, MRLB-45696-treated *Sco2*^{KOKI}. Paired, two-tailed Student's t test; **p < 0.01.

(B) NAD+ concentration in skeletal muscle. Solid black, vehicle-treated WT; black outline, MRLB-45696-treated WT; solid red, vehicle-treated *Sco2*^{KOKI}; red outline, MRLB-45696-treated *Sco2*^{KOKI}. Error bars represent SD. Unpaired, two-tailed Student's t test; *p < 0.05.

(C) Analysis of acetylation of FOXO1. Both WT and *Sco2*^{KOKI} samples showed reduced acetylation and increased total FOXO1 upon MRLB-45696 treatment, indicating activation of Sirt1. Tubulin was taken as loading control. Densitometric analysis is presented in Table S3.

(D) mRNA expression analysis of FAO- and OXPHOS-related genes in *Sco2*^{KOKI} and WT muscles of NR-treated and vehicle-treated mice. Solid black, vehicle-treated WT; black outline, MRLB-45696-treated WT; solid red, vehicle-treated *Sco2*^{KOKI}; red outline, MRLB-45696-treated *Sco2*^{KOKI}. Gene transcripts, retrotranscribed into cDNA, were normalized to the *Hprt* gene transcript, taken as a standard, and expressed as time fold variation relative to the WT. Error bars represent SD. Unpaired, two-tailed Student's t test; *p < 0.05; **p < 0.01; ***p < 0.001.

(E) Western blot immunovisualization of COX1, COXVa, SDH 70KDa, Core 2, 39 KDa complex I subunit proteins in skeletal muscle of MRLB-45696-treated and vehicle-treated mice of the different genotypes. Note the increased amount of respiratory chain subunits in MRLB-45696-treated *Sco2*^{KOKI} samples.

(F) Respiratory chain activities (nmoles/min/mg of protein). Color codes as in (B). CS, citrate synthase; CI-IV, MRC complexes I–IV. Error bars represent SD. Unpaired, two-tailed Student's t test; **p < 0.01; ***p < 0.001.

(G) COX staining in skeletal muscles of (Ga) vehicle-treated WT, (Gb) MRLB-45696-treated WT, (Gc) vehicle-treated *Sco2*^{KOKI}, and (Gd) MRLB-45696-treated *Sco2*^{KOKI}. Scale bar, 100 μm.

(H) mRNA expression analysis of mtUPR genes *Hsp60*, *Clpp*, and *Sod2* in *Sco2*^{KOKI} and WT muscles of MRLB-45696-treated and vehicle-treated mice. *Sod3* was taken as a non-mtUPR related stress protein. Color codes as in (B). The levels of the gene transcripts, retrotranscribed into cDNA, were normalized to that of the *Hprt* gene transcript, taken as a standard, and expressed as time fold variation relative to the WT. Error bars represent SD. Unpaired, two-tail Student's t test; **p < 0.01.

muscle and possibly other tissues to activators of mitochondriogenic programs. Increased mitochondrial function can be achieved in WT animals only by much longer-term treatments (>6 months) (Pirinen et al., 2014).

In contrast with previous results, we found no change in mtDNA copy number and CS activity in NR- or PARPi-treated versus untreated animals, possibly because of the shorter timeframe of our experimental protocol (4 weeks) compared to that of other studies (12 weeks). This observation suggests time-dependent activation of different mitochondriogenic programs, with induction of OXPHOS- and FAO-related genes occurring much earlier than stimulation of mitochondrial proliferation and

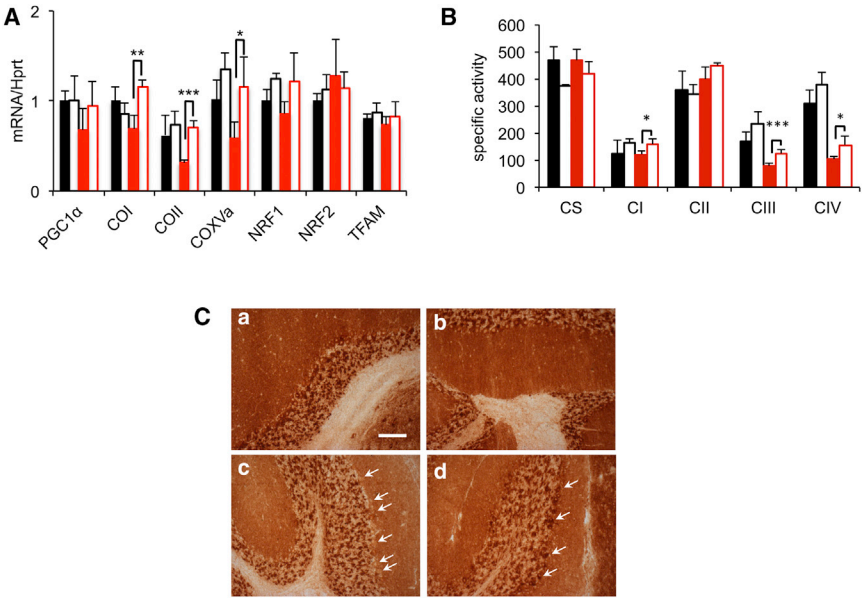

Figure 4. Effect of MRLB-45696 in the Brain

(A) mRNA expression analysis in the brain. Solid black, vehicle-treated WT; black outline, MRLB-45696-treated WT; solid red, vehicle-treated *Sco2*^{KOKI}; red outline, MRLB-45696-treated *Sco2*^{KOKI}.

(B) Respiratory chain activities (nmoles/min/mg of protein). Color codes as in (A). CS, citrate synthase; CI-IV, MRC complexes I–IV. Error bars represent SD. The asterisks represent the significance levels calculated by unpaired, two-tailed Student's t test; **p < 0.01; ***p < 0.001.

(C) COX staining in the brain of MRLB-45696 treated and vehicle-treated *Sco2*^{KOKI} and WT mice. The arrows indicate Purkinje cells showing increased COX activity. Scale bar, 100 μm.

increase in mtDNA content. Likewise, prolonged NR supplementation up to 6 months induced mitochondrial biogenesis in the brain and improvement of cognitive dysfunction of an Alzheimer disease mouse model (Gong et al., 2013). While we observed hardly any effect of NR in our 4 week trial, two pan-PARP inhibitors did correct the respiratory chain defect in the brains of our *Sco2*^{KOKI} mice. This observation is particularly relevant, as the brain is an exquisite target of mitochondrial dysfunction, and progressive encephalopathy is the most frequent clinical presentation of mitochondrial disease in infancy and childhood.

Our work supports the idea that the increase of NAD^+ levels in critical tissues is an effective therapeutic option for mitochondrial disease. NR is a natural vitamin with no known adverse effects, which could be administered as a dietary supplement, particularly in case of isolated mitochondrial myopathy. Our results are concordant with very recent works reporting beneficial effects of NAD^+ precursors in mouse models characterized by reduced NAD^+/NADH ratio, such as aging (Gomes et al., 2013) or complex I deficiency (Karamanlidis et al., 2013).

The therapeutic potential of Parp inhibitors has recently attracted much interest. Initially shown to boost oxidative metabolism in diet-induced models of obesity, Parp1 ablation or inhibition has recently been reported to remarkably rescue pharmacological models of liver cirrhosis, partly by correcting the associated mitochondrial impairment (Mukhopadhyay et al., 2013). Several PARP inhibitors are currently under clinical trial as anticancer molecules, and seem to be associated with relatively mild side effects (Bundred et al., 2013; Tutt et al., 2010). However, more work is needed to evaluate their use in chronic conditions such as primary mitochondrial disorders in view of their potential genotoxic effects.

EXPERIMENTAL PROCEDURES

Western Blot Analysis

Mouse tissues were homogenized in 15 volumes of 10 mM potassium phosphate buffer (pH 7.5). Mitochondrial-enriched fractions were collected after centrifugation at 800 g for 10 min in the presence of protease inhibitors, and frozen and thawed three times in liquid nitrogen. Protein concentration was determined by the Lowry method. Aliquots, 70 μg each, were run through a 12% SDS-PAGE and electroblotted onto a nitrocellulose membrane, which was then matched with different antibodies.

In Vivo Experiments

Animal studies were approved by the Ethics Committee of the Foundation "Carlo Besta" Neurological Institute, in accordance with guidelines of the Italian Ministry of Health. The use and care of animals followed the Italian Law D.L. 116/1992 and the EU directive 86/609/CEE. Mice were maintained in a temperature- and humidity-controlled animal-care facility, with a 12 hr light/dark cycle and free access to water and food. Animals were sacrificed by cervical dislocation.

Locomotor Analysis

A standard treadmill apparatus (Columbus Instruments, Columbus, OH) was used to measure motor exercise endurance, as described in Viscomi et al. (2011)

Morphological Analysis

For histochemical analysis, tissues were frozen in liquid-nitrogen precooled isopentane. Series of 8 μm thick sections were stained for COX and SDH, as described (Sciacco and Bonilla, 1996).

Biochemical Analysis of MRC Complexes

Muscle quadriceps samples stored in liquid nitrogen were homogenized in 10 mM phosphate buffer (pH 7.4), and the spectrophotometric activity of cI, cII, cIII, and cIV, as well as CS, was measured as described (Bugiani et al., 2004). Note that in all panels the activity of cII has been multiplied by 10 for visualization clarity.

NAD^+ Determination

NAD^+ was extracted using acidic and alkaline extraction methods, respectively (Yang and Sauve, 2006). Tissue NAD^+ was analyzed with mass spectrometry as previously described (Yang and Sauve, 2006).

Real-Time PCR

MtDNA content and transcripts analysis was carried out by SYBR Green real-time PCR, as described (Viscomi et al., 2011).

SUPPLEMENTAL INFORMATION

Supplemental Information includes Supplemental Experimental Procedures, four figures, and four tables and can be found with this article at http://dx.doi.org/10.1016/j.cmet.2014.04.001.

ACKNOWLEDGMENTS

This work was supported by the Pierfranco and Luisa Mariani Foundation Italy, Telethon-Italy GPP10005 and GGP11011 (to M.Z.), Cariplo 2011-0526, ERC FP7-322424 (to M.Z.), and GR-2010-2306-756 (to C.V.); and by grants of the Ecole Polytechnique Fédérale de Lausanne (to J.A.), the EU Ideas program (ERC-2008-AdG-23138 to J.A.), the NIH (R01HL106511-01A and R01AG043930 to J.A.), the Velux Stiftung, and the Swiss National Science Foundation (31003A-124713 and 31003A-125487 to J.A.). J.A. is the Nestlé Chair in Energy Metabolism. E.A.S. is supported by: the National Institutes of Health (HD32062), the U.S. Department of Defense (W911NF-12-1-0159), the Muscular Dystrophy Association, the Ellison Medical Foundation, and the J. Willard and Alice S. Marriott Foundation; A.A.S. is supported by the National Institutes of Health (1R01GM106072-01).

Received: October 14, 2013
Revised: January 17, 2014
Accepted: March 14, 2014
Published: May 8, 2014

REFERENCES

Adamietz, P. (1987). Poly(ADP-ribose) synthase is the major endogenous nonhistone acceptor for poly(ADP-ribose) in alkylated rat hepatoma cells. Eur. J. Biochem. *169*, 365–372.

Andreux, P.A., Houtkooper, R.H., and Auwerx, J. (2013). Pharmacological approaches to restore mitochondrial function. Nat. Rev. Drug Discov. *12*, 465–483.

Bai, P., Cantó, C., Oudart, H., Brunyánszki, A., Cen, Y., Thomas, C., Yamamoto, H., Huber, A., Kiss, B., Houtkooper, R.H., et al. (2011). PARP-1 inhibition increases mitochondrial metabolism through SIRT1 activation. Cell Metab. *13*, 461–468.

Bieganowski, P., and Brenner, C. (2004). Discoveries of nicotinamide riboside as a nutrient and conserved NRK genes establish a Preiss-Handler independent route to NAD+ in fungi and humans. Cell *117*, 495–502.

Bugiani, M., Invernizzi, F., Alberio, S., Briem, E., Lamantea, E., Carrara, F., Moroni, I., Farina, L., Spada, M., Donati, M.A., et al. (2004). Clinical and molecular findings in children with complex I deficiency. Biochim. Biophys. Acta *1659*, 136–147.

Bundred, N., Gardovskis, J., Jaskiewicz, J., Eglitis, J., Paramonov, V., McCormack, P., Swaisland, H., Cavallin, M., Parry, T., Carmichael, J., and Dixon, J.M. (2013). Evaluation of the pharmacodynamics and pharmacokinetics of the PARP inhibitor olaparib: a phase I multicentre trial in patients scheduled for elective breast cancer surgery. Invest. New Drugs *31*, 949–958.

Cantó, C., and Auwerx, J. (2009). Caloric restriction, SIRT1 and longevity. Trends Endocrinol. Metab. *20*, 325–331.

Cantó, C., and Auwerx, J. (2010). Clking on PGC-1alpha to inhibit gluconeogenesis. Cell Metab. *11*, 6–7.

Cantó, C., Houtkooper, R.H., Pirinen, E., Youn, D.Y., Oosterveer, M.H., Cen, Y., Fernandez-Marcos, P.J., Yamamoto, H., Andreux, P.A., Cettour-Rose, P., et al. (2012). The NAD(+) precursor nicotinamide riboside enhances oxidative metabolism and protects against high-fat diet-induced obesity. Cell Metab. *15*, 838–847.

Chen, D., Bruno, J., Easlon, E., Lin, S.J., Cheng, H.L., Alt, F.W., and Guarente, L. (2008). Tissue-specific regulation of SIRT1 by calorie restriction. Genes Dev. *22*, 1753–1757.

de Murcia, J.M., Niedergang, C., Trucco, C., Ricoul, M., Dutrillaux, B., Mark, M., Oliver, F.J., Masson, M., Dierich, A., LeMeur, M., et al. (1997). Requirement of poly(ADP-ribose) polymerase in recovery from DNA damage in mice and in cells. Proc. Natl. Acad. Sci. USA *94*, 7303–7307.

Durieux, J., Wolff, S., and Dillin, A. (2011). The cell-non-autonomous nature of electron transport chain-mediated longevity. Cell *144*, 79–91.

Durkacz, B.W., Omidiji, O., Gray, D.A., and Shall, S. (1980). (ADP-ribose)n participates in DNA excision repair. Nature *283*, 593–596.

Gomes, A.P., Price, N.L., Ling, A.J., Moslehi, J.J., Montgomery, M.K., Rajman, L., White, J.P., Teodoro, J.S., Wrann, C.D., Hubbard, B.P., et al. (2013). Declining NAD(+) induces a pseudohypoxic state disrupting nuclear-mitochondrial communication during aging. Cell *155*, 1624–1638.

Gong, B., Pan, Y., Vempati, P., Zhao, W., Knable, L., Ho, L., Wang, J., Sastre, M., Ono, K., Sauve, A.A., and Pasinetti, G.M. (2013). Nicotinamide riboside restores cognition through an upregulation of proliferator-activated receptor-γ coactivator 1α regulated β-secretase 1 degradation and mitochondrial gene expression in Alzheimer's mouse models. Neurobiol. Aging *34*, 1581–1588.

Houtkooper, R.H., Cantó, C., Wanders, R.J., and Auwerx, J. (2010). The secret life of NAD+: an old metabolite controlling new metabolic signaling pathways. Endocr. Rev. *31*, 194–223.

Houtkooper, R.H., Pirinen, E., and Auwerx, J. (2012). Sirtuins as regulators of metabolism and healthspan. Nat. Rev. Mol. Cell Biol. *13*, 225–238.

Imai, S., Armstrong, C.M., Kaeberlein, M., and Guarente, L. (2000). Transcriptional silencing and longevity protein Sir2 is an NAD-dependent histone deacetylase. Nature *403*, 795–800.

Karamanlidis, G., Lee, C.F., Garcia-Menendez, L., Kolwicz, S.C., Jr., Suthammarak, W., Gong, G., Sedensky, M.M., Morgan, P.G., Wang, W., and Tian, R. (2013). Mitochondrial complex I deficiency increases protein acetylation and accelerates heart failure. Cell Metab. *18*, 239–250.

Koopman, W.J., Willems, P.H., and Smeitink, J.A. (2012). Monogenic mitochondrial disorders. N. Engl. J. Med. *366*, 1132–1141.

Leary, S.C., Sasarman, F., Nishimura, T., and Shoubridge, E.A. (2009). Human SCO2 is required for the synthesis of CO II and as a thiol-disulphide oxidoreductase for SCO1. Hum. Mol. Genet. *18*, 2230–2240.

Mouchiroud, L., Houtkooper, R.H., Moullan, N., Katsyuba, E., Ryu, D., Cantó, C., Mottis, A., Jo, Y.S., Viswanathan, M., Schoonjans, K., et al. (2013). The NAD(+)/sirtuin pathway modulates longevity through activation of mitochondrial UPR and FOXO signaling. Cell *154*, 430–441.

Mukhopadhyay, P., Rajesh, M., Cao, Z., Horváth, B., Park, O., Wang, H., Erdelyi, K., Holovac, E., Wang, Y., Liaudet, L., et al. (2013). Poly (ADP-ribose) polymerase-1 is a key mediator of liver inflammation and fibrosis. Hepatology. Published online April 1, 2014. http://dx.doi.org/10.1002/hep.26763.

Papadopoulou, L.C., Sue, C.M., Davidson, M.M., Tanji, K., Nishino, I., Sadlock, J.E., Krishna, S., Walker, W., Selby, J., Glerum, D.M., et al. (1999). Fatal infantile cardioencephalomyopathy with COX deficiency and mutations in SCO2, a COX assembly gene. Nat. Genet. *23*, 333–337.

Peek, C.B., Affinati, A.H., Ramsey, K.M., Kuo, H.Y., Yu, W., Sena, L.A., Ilkayeva, O., Marcheva, B., Kobayashi, Y., Omura, C., et al. (2013). Circadian clock NAD+ cycle drives mitochondrial oxidative metabolism in mice. Science *342*, 1243417.

Pirinen, E., Cantó, C., Jo, Y.S., Morato, L., Zhang, H., Menzies, K.J., Williams, E.G., Mouchiroud, L., Moullan, N., Hagberg, C., et al. (2014). Pharmacological inhibition of poly(ADP-ribose) polymerases improves fitness and mitochondrial function in skeletal muscle. Cell Metab. *19*. Published online May 8, 2014. http://dx.doi.org/10.1016/j.cmet.2014.04.002.

Rodgers, J.T., Lerin, C., Haas, W., Gygi, S.P., Spiegelman, B.M., and Puigserver, P. (2005). Nutrient control of glucose homeostasis through a complex of PGC-1alpha and SIRT1. Nature *434*, 113–118.

Sciacco, M., and Bonilla, E. (1996). Cytochemistry and immunocytochemistry of mitochondria in tissue sections. Methods Enzymol. *264*, 509–521.

Tutt, A., Robson, M., Garber, J.E., Domchek, S.M., Audeh, M.W., Weitzel, J.N., Friedlander, M., Arun, B., Loman, N., Schmutzler, R.K., et al. (2010). Oral poly(ADP-ribose) polymerase inhibitor olaparib in patients with BRCA1 or BRCA2 mutations and advanced breast cancer: a proof-of-concept trial. Lancet *376*, 235–244.

Vaziri, H., Dessain, S.K., Ng Eaton, E., Imai, S.I., Frye, R.A., Pandita, T.K., Guarente, L., and Weinberg, R.A. (2001). hSIR2(SIRT1) functions as an NAD-dependent p53 deacetylase. Cell *107*, 149–159.

Viscomi, C., Bottani, E., Civiletto, G., Cerutti, R., Moggio, M., Fagiolari, G., Schon, E.A., Lamperti, C., and Zeviani, M. (2011). In vivo correction of COX deficiency by activation of the AMPK/PGC-1α axis. Cell Metab. *14*, 80–90.

Wenz, T., Diaz, F., Spiegelman, B.M., and Moraes, C.T. (2008). Activation of the PPAR/PGC-1alpha pathway prevents a bioenergetic deficit and effectively improves a mitochondrial myopathy phenotype. Cell Metab. *8*, 249–256.

Yang, T., and Sauve, A.A. (2006). NAD metabolism and sirtuins: metabolic regulation of protein deacetylation in stress and toxicity. AAPS J. *8*, E632–E643.

Yang, H., Brosel, S., Acin-Perez, R., Slavkovich, V., Nishino, I., Khan, R., Goldberg, I.J., Graziano, J., Manfredi, G., and Schon, E.A. (2010). Analysis of mouse models of cytochrome c oxidase deficiency owing to mutations in Sco2. Hum. Mol. Genet. *19*, 170–180.